Biomedical Materials

CrossMark

RECEIVED
24 September 2018

REVISED
14 January 2019

ACCEPTED FOR PUBLICATION
12 February 2019

PUBLISHED
26 March 2019

PAPER

Use of cerium oxide nanoparticles: a good candidate to improve skin tissue engineering

Atefeh Pesaraklou[1], **Nasser Mahdavi-Shahri**[1], **Halimeh Hassanzadeh**[1,2], **Masoud Ghasemi**[1], **Mahboubeh Kazemi**[1], **Nasser Sanjar Mousavi**[3] **and Maryam M Matin**[1,2,4]

[1] Department of Biology, Faculty of Science, Ferdowsi University of Mashhad, Mashhad, Iran
[2] Stem Cells and Regenerative Medicine Research Group, Academic Center for Education, Culture, and Research (ACECR), Khorasan Razavi Branch, Mashhad, Iran
[3] Department of Surgery, Faculty of Medicine, Islamic Azad University-Mashhad Branch, Mashhad, Iran
[4] Novel Diagnostics and Therapeutics Research Group, Institute of Biotechnology, Ferdowsi University of Mashhad, Mashhad, Iran

E-mail: matin@um.ac.ir

Keywords: cerium oxide nanoparticles, adipose-derived mesenchymal stem cells, acellular dermal matrix, proliferation, tissue engineering

Abstract

Today advancements in nanotechnology have made extensive progress in tissue engineering. Application of cerium oxide nanoparticles (CeO_2) has improved regenerative medicine due to their antioxidant properties. In this study, nanoparticles were used to increase the efficacy of skin substitutes. Human skin samples were decellularized using four methods and studied via histological stainings and DNA content analyses. Then CeO_2 dispersing and its stability were investigated. The prepared acellular dermal matrices (ADMs) were immersed in CeO_2 suspension and their effects were evaluated on growth of cultured human adipose derived-mesenchymal stem cells (hAd-MSCs) using 3-(4,5-dimethylthiazol-2-yl)-2,5-diphenyltetrazolium bromide (MTT) assay and histological methods. Moreover, their antioxidant properties were assessed based on DPPH degradation. Changes in the collagen contents of the scaffolds containing cells and CeO_2 were also determined by electron microscopy and their tensile strength was compared to ADM. Our results indicated that use of trypsin/NaOH protocol resulted in most efficient cell removal while maintaining extracellular matrix (ECM) architecture. Among different dispersal methods, the approach using Dulbecco's modified Eagle's medium (DMEM), wetting with fetal bovine serum (FBS) and ultrasonic bath resulted in the best stability. Furthermore, it was shown that CeO_2 not only had no toxicity on the cells, but also increased the growth and survival of hAd-MSCs by about 27%, improved free radical scavenging, as well as the amount of collagen and tensile strength of the scaffolds containing nanoparticles compared to the ADM. It can be concluded that the combination of ADM/CeO_2/hAd-MSCs could be a step forward in skin tissue engineering.

Abbreviations

ADM	acellular dermal matrix
Ad-MSCs	adipose-derived mesenchymal stem cells
CeO_2	cerium oxide
DAPI	4, 6-Diamidino-2-phenylindole
DMEM	Dulbecco's modified Eagle's medium
DMSO	dimethyl sulfoxide
DPPH	2, 2-diphenyl-1-picrylhydrazyl
ECM	extracellular matrix
EDTA	ethylenediaminetetraacetic acid
FBS	fetal bovine serum
MTT	3-(4,5-dimethylthiazol-2-yl)-2,5-diphenyl tetrazolium bromide
OD	optical density

PBS	phosphate buffered saline
SEM	scanning electron microscope
TEM	transmission electron microscope

1. Introduction

Skin is important because of various sensory, protective and metabolic functions. Although in surface damages, the skin naturally repairs itself, in deep wounds, the healing process is disrupted [1]. In such a situation, different methods are used to improve the treatment outcome. These methods include use of soluble molecules such as growth factors, gene targeting, stem cell therapy, tissue engineering, cellular reprogramming, protein delivery, biomimetic scaffolds and other medical devices [2, 3]. Regenerative medicine is rapidly growing as a new discipline in biomedical research and focuses on the replacement and regeneration of damaged cells, tissues and organs [4]. Tissue engineering is an interdisciplinary field in medical sciences, which use suitable growth factors and extracellular matrices (as scaffolds) to support cell growth [5].

Ad-MSCs are a population of multipotent mesenchymal stem cells that can be differentiated into a variety of cell types. For some time, Ad-MSCs have been studied extensively in rehabilitation medicine and tissue engineering due to their secretion of regenerative growth factors, differentiation capacity, immunomodulatory effects, and migration to the site of injury [6].

Decellularized matrices provide a natural microenvironment for cellular adhesion and proliferation. They promote processes such as angiogenesis, cell division and have even shown antimicrobial activities [7, 8]. It should be noted that the variability of the extracellular matrix structure at different stages of preparation might affect the interaction of the matrix with the host [9]. So the preparation of these matrices should be done with great accuracy.

In recent years, with the advent of nanotechnology, regenerative medicine has progressed and combination of these methods seems to be a promising approach in restoring the function and repair of damaged tissues and organs [10]. In most cases, the physical, chemical, and biological properties of nanoscale materials indicate differences in comparison with bulk. Nanoparticles are materials of less than 100 nanometers in all three dimensions [11]. CeO_2 nanoparticles are considered as a scavenger for free radicals (antioxidant) [12, 13] Applications of these nanoparticles in biomedicine include: anti-inflammation [14], protection against laser ocular lesions [15], protection against radiation-induced tissue damage [16, 17], induction of angiogenesis and wound healing [18–21], reduction of neurological diseases [22–25], anti-angiogenesis and inhibiting of tumor invasion [26–28], bone tissue engineering [20] and others [29].

In this study, first we attempted to produce a decellularized matrix of human skin with the most cell removal and minimal damage to the ECM. Then we studied different methods for cerium oxide nanoparticles (CeO_2) dispersion and the amount of nanoparticles taken up by the ADM was determined based on photoluminescence of free CeO_2 nanoparticles. Antioxidant activities of ADM and ADM/CeO_2 were determined by DPPH assay. Finally, we investigated the effects of CeO_2 on viability and growth of hAd-MSCs seeded on ADM/CeO_2 with MTT assay and collagen density and their alignment were studied using histological stainings and electron microscopy. Furthermore, the effects of CeO_2 on improving mechanical properties of these skin substitutes were determined by tensile test.

2. Materials and methods

2.1. Materials

Cerium oxide (CeO_2) nanoparticle powder (US Research Nanomaterials, Inc.). Trizol, Dulbecco's modified Eagle's medium (DMEM), fetal bovine serum (FBS) and trypsin/EDTA solution were acquired from Gibco (Germany). Phosphate buffered saline (PBS) was obtained from DENA Zist Asia (Iran), and sodium dodecyl sulfate (SDS), Triton X-100 and absolute ethanol were purchased from Merck (Germany).

2.2. CeO_2 nanoparticles dispersion

In present study, the aqueous suspension of CeO_2 nanoparticles was used. In order to achieve a homogeneous suspension, nanoparticle powder was dispersed in various conditions including different media (PBS, ddH_2O and DMEM), pH (acidic and physiologic) and CeO_2 concentrations (1 and 20 mg ml^{-1}) as well as wetting with FBS and water.

2.3. Zeta potential and particle size measurements

Nanoparticle suspensions with a significant deposition and color variation were discarded from further analysis. The stability of other suspensions were measured at 0 and 24 h time intervals after dispersion using a Particle Size Analyzer (Vasco3—Cordouan—France) and Zeta meter (Zeta Compact—CAB—France), which uses a laser with the wavelength of 633 nm.

2.4. Optical properties of dispersed CeO_2

Photoluminescence and UV–visible spectroscopy were performed to evaluate optical properties and obtain excitation and emission wavelengths of our CeO_2 nanoparticles. Subsequently, the photoluminescence (PL) was recorded by a spectero fluorophotometer (Perkinelmer Is 45. US).

2.5. Preparation of human acellular dermal matrix (hADM)

Human skin samples were obtained after liposuction surgery. After several washes with physiological serum, skin samples were cut into 0.5 × 0.5 or 0.5 × 2.5 cm^2 pieces as required. The ADM should be able to provide a natural microenvironment for cellular adhesion and proliferation. Different decellularization methods including: treatment with NaCl/Triton X-100 or SDS [30], trypsin/Triton X-100 [31] and trypsin/NaOH [32] were applied. At the end of all treatments, the scaffolds were washed with PBS to remove the remaining detergents completely. The samples prepared using the best protocol were finally lyophilized using a freeze-dryer (Christ-Germany).

2.6. DNA content

A comparison was made between DNA content in the intact and ADM samples prepared using trypsin/NaOH protocol. In order to quantify the efficacy of cell removal, DNA extraction was performed using TRIzol according to manufacturer's instructions using 80 mg of fresh samples. To determine the concentration of DNA, optical density of samples were read at 260 and 280 nm wavelengths using a nanodrop (Thermo Scientific, US).

2.7. Immersing ADMs in CeO_2 suspension

In order to test the effects of CeO_2 nanoparticles, scaffolds prepared using trypsin/NaOH as the best decellularization method were immersed in nanoparticles. Zeta potential and particle size measurements indicated that use of ultrasound bath and FBS was the best protocol for preparation of CeO_2 suspension. ADMs were placed in suspensions of nanoparticles with different concentrations for 24 h. For better penetration of nanoparticles into the scaffolds, this step was performed in a shaker-incubator at 37 °C and 230 rpm. Agglomerated nanoparticles were also washed with sterile PBS. Before cell seeding on ADM/CeO_2, these scaffolds were sterilized with 70% ethanol for 20 min followed by incubation with sterile PBS containing penicillin (10000 units ml^{-1}) streptomycin (10000 $\mu g\ ml^{-1}$) antibiotics for 1 h. To determine the amount of nanoparticles taken up by the ADM, different concentrations of CeO_2 NPs (0.25, 0.5, 0.75, 1, 1.5 and 2 mg ml^{-1}) were prepared and standard curve was created (excitation wavelength = 342 nm). Standard curve determines the relationship between two quantities (PL and CeO_2 concentrations). ADMs were immersed in CeO_2 suspension (1 mg ml^{-1} CeO_2) followed by measuring PL after 24 h of immersion. Finally, the amount of nanoparticles taken up by the ADM was calculated.

2.8. Antioxidant activity assay

Antioxidant properties of the acellular dermal matrix (without nanoparticles and containing different concentrations of CeO_2) were assessed by 2,2-diphenyl-1-picrylhydrazyl (DPPH) assay. ADM and ADM/CeO_2 were placed into wells of 48 well plates. 1 ml of 100 μM DPPH solution was added to each well and incubated for 90 min in dark. DPPH free radical content was measured by monitoring the changes in the absorbance at 517 nm by a UV–vis spectrophotometer (unico, S2100UV) [33].

DPPH degradation was calculated using the following formula:

$$\text{Percentage of DPPH scavenging} = \frac{\text{absorbance of blank} - \text{absorbance of sample}}{\text{absorbance of blank}} \times 100$$

2.9. Derivation and culture of hAd-MSCs

Human adipose-derived mesenchymal stem cells (MSCs) were isolated from adipose tissues obtained through liposuction surgery. MSCs isolation and characterization were carried out as reported previously [34]. Cells were cultured in DMEM supplemented with 10% FBS and 1% penicillin-streptomycin. Cultures were incubated in a humidified atmosphere containing 5% CO_2 at 37 °C with a change of culture medium once every other day.

2.10. Histological studies

Efficacy of different decellularization protocols on cell removal and maintenance of ECM integrity as well as, the effects of CeO_2 on ECM components and the interactions of cultured Ad-MSCs on human ADM, were studied using histological methods. All samples were fixed in 4% formaldehyde and processed by a tissue processor (DID SABZ CO, Iran). After embedding, thin slices of tissues (5–7 μm) were prepared using a microtome (Leitz, Austria). In the next step, samples were deparaffinized by xylen and then descending ethanol grades were used to increase dye penetration into tissue samples. H&E and varius specific stainings (Picro sirius red, Van Gieson, Picro—indigo carmine and 4,6-Diamidino-2-phenylindole (DAPI) stainings) were then applied as required.

2.11. MTT assay for hAd-MSCs

The effects of CeO_2 on survival of hAd-MSCs were examined by MTT assay. For this purpose, hAd-MSCs were seeded in three 96 well plates at a concentration of 6000 cells per 200 μl of culture medium. When the cells reached 70% confluency, they were treated with different concentrations of CeO_2 ranging from 17×10^{-6} to 170 $\mu g\ ml^{-1}$ for 24, 48 and 72 h. In order to determine cell survival, 20 μl MTT solution was added to each well and cells were incubated at 37 °C for 3 h. The media containing MTT solution were replaced with 150 μl dimethyl sulfoxide (DMSO) to dissolve the insoluble formazan crystals and the absorbances were measured at 545 nm using an ELISA (enzyme-linked immunosorbent assay) reader (Awareness Technology Inc.—US).

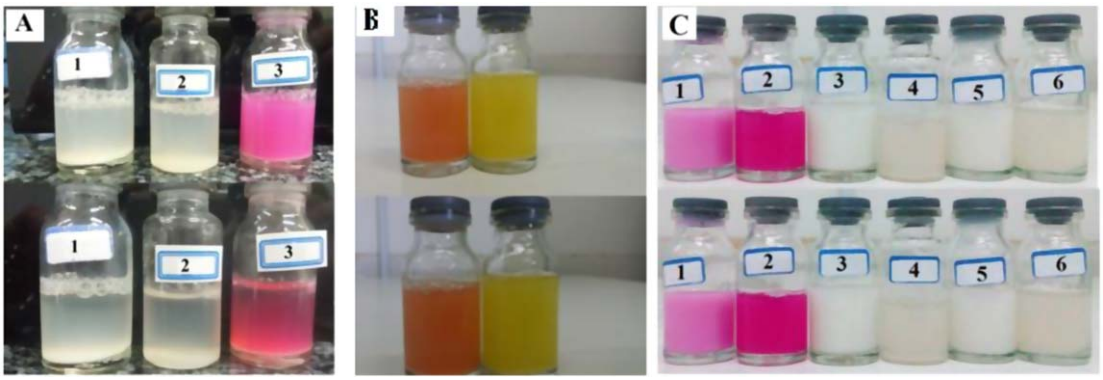

Figure 1. Dispersion of CeO_2 in different media, without FBS (A): (1) ddH_2O (2) PBS (3) DMEM. Discoloration created duo to precipitation indicates the instability of the prepared suspensions. (B) In acidic pH apparent stability is observed (C). Different media including: (1), (2) DMEM + 10% FBS, (3), (4) PBS + 10% FBS (5,6) ddH_2O + 10% FBS containing different concentrations of CeO_2: (1), (3), (5) 20 mg ml^{-1}, (2), (4), (6) 1 mg ml^{-1}.

2.12. MTT assay for ADM/CeO_2/hAd-MSCs

Prepared ADM/CeO_2 constructs ($0.5 \times 0.5\ cm^2$) were placed into three 48 well plates. 1×10^5 hAd-MSCs per 40 μl were seeded onto each scaffold and left for 1 h for cells to attach to the scaffolds. Then, 800 μl of culture medium was added to each well and incubated at 37 °C and 5% CO_2. Media were changed every other day. Viability and growth of cultivated cells on the scaffolds were evaluated after 12 h and also at days 3, 7 and 14 by MTT assay as described previously.

2.13. Scanning electron microscopy

Topology comparison between ADM, ADM/Ad-MSCs and ADM/CeO_2/Ad-MSCs as well as adhesion, growth and morphology of cells on the dermis scaffolds were studied using SEM (VP 1450, LEO—Germany). Samples were fixed in glutaraldehyde, dehydrated with ethanol and dried in air. Finally, all scaffolds were coated with gold-palladium and studied by SEM.

2.14. Transmission electron microscopy (TEM)

In order to investigate the effects of CeC_2 on collagen arrangement and orientation, we used TEM. Samples were fixed in glutaraldehyde, dehydrated with ethanol and an ultramicrotome (Leica EM UC7, Austria) was used to make 80 nm slices of tissues. Finally, after staining with uranyl acetate and lead citrate, samples were examined using TEM (AB 912, LEO—Germany).

2.15. Tensile test

The comparison of the mechanical properties between ADM, ADM/Ad-MSCs and ADM/CeO_2/Ad-MSCs ($0.5 \times 2.5\ cm^2$) was performed by measuring elasticity strength of the samples at Dental Materials Laboratory of Mashhad University of Medical Sciences. For this purpose, constructs were placed into 6 well plates and 5×10^5 hAd-MSCs were seeded onto each scaffold and incubated for different time points. To do the test, samples were placed between two grips of testing machine (SANT-M, Iran). Measurements of tensile strength and elongation at break were obtained from stress–strain curves at days 3, 7 and 14 after seeding.

2.16. Statistical analyses±

All results were analyzed using GraphPad Prism v6.07 software. Results are expressed as mean, ±SD. Statistical comparisons between two groups were made using the Student's *t*-test, while multiple comparisons were made using two-way analysis of variance (ANOVA). Moreover, Dunnett test was adopted to compare every mean to a control mean after ANOVA and $p < 0.05$ was considered to be statistically significant.

3. Results

3.1. Stability of dispersed CeO_2 nanoparticles

Different protocols of dispersion were used to achieve the most stable suspensions for CeO_2 nanoparticles. When samples were prepared by wetting with water and dispersed using ultrasonic bath the formation of sediment in the early hours (figure 1), resulted in elimination of this protocol from the continuation of the study. When citric acid was used as a stabilizer, the suspensions had apparent stability but were not suitable for use in biological systems. The dispersed nanoparticles in deionized water, PBS and DMEM using vortex and sonication bath were apparently stable for 24 h. The results of zeta potential measurement and particle size (table 1) indicated that nanoparticles had the highest stability in DMEM. Moreover, when FBS was used for wetting, the zeta potential was negatively affected and the particle size became smaller and thus more stable.

3.2. Evaluating excitation and emission wavelengths of CeO_2 suspension

In order to evaluate optical properties of nanoparticles after dispersion, photoluminescence and UV–visible

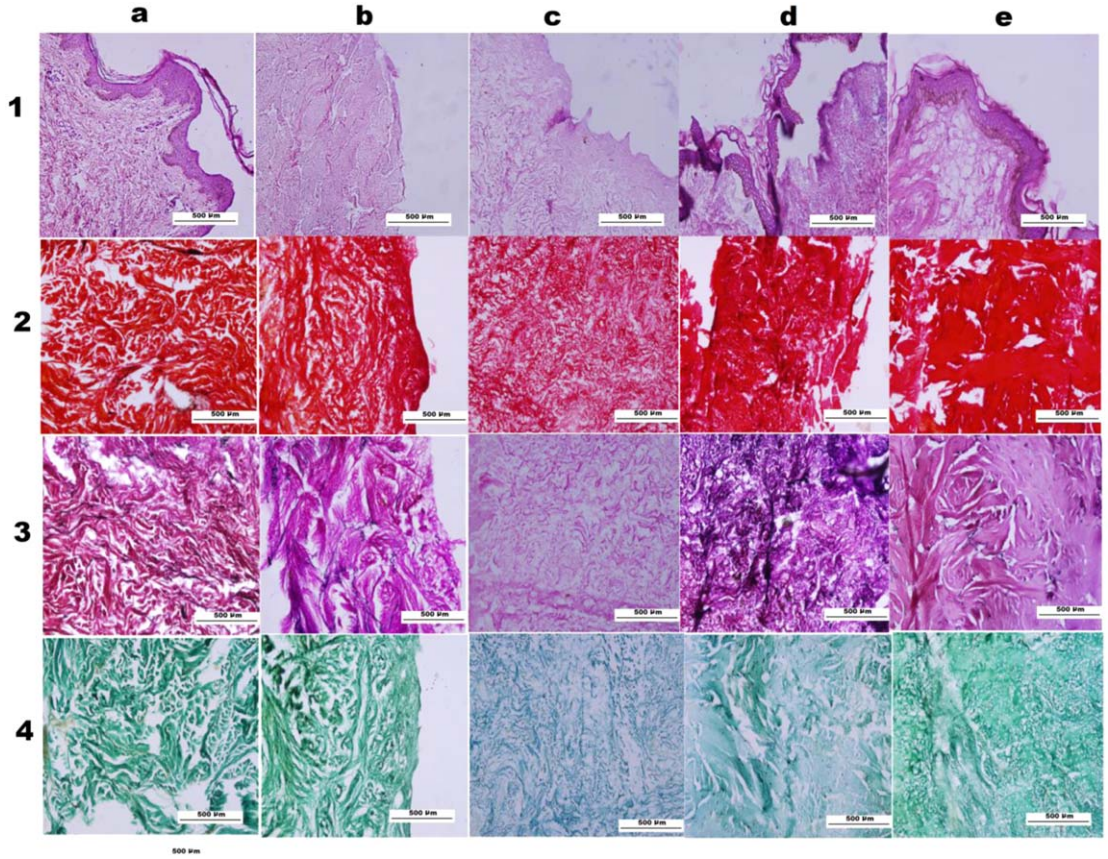

Figure 2. Investigating the efficacy of decellularization by histological methods. H&E staining of control and decellularized samples are shown in (1). Samples were stained with Picro sirius red (2), Van Gieson (3) and Picro-indigo carmine (4) in order to check the integrity of the ECM. Controls (a) are shown along with representative samples decellularized with different methods including trypsin/NaOH (b), NaCl/SDS (c), trypsin/Triton X-100 (d) and NaCl/Triton X-100 (e). H&E images show a better cell removal in micrographs (c) and (e), and the least changes in the structure of collagens were observed in the scaffolds prepared with trypsin/NaOH as compared with control skin samples. Scale bar 500 μm.

Table 1. The results of zeta potential and CeO_2 particle size after using different methods for dispersion, as measured at different time points.

Medium	Method	Zeta potential after 1 h	Zeta potential after 24 h	Particle size after 1 h (nm)	Particle size after 24 h (nm)
ddH_2O	Ultrasonic	-17 ± 1	-20 ± 1	260 ± 20	150 ± 20
PBS	Ultrasonic	-24 ± 1	-23 ± 1	200 ± 10	210 ± 20
DMEM	Ultrasonic	-27 ± 2	-26 ± 2	100 ± 20	110 ± 20
DMEM	Wetting with FBS	-34 ± 2	-33 ± 2	110 ± 20	80 ± 20
DMEM	Probe sonic	-31 ± 1	-30 ± 1	110 ± 10	70 ± 20

spectroscopy were used. Excitation and emission wavelengths for CeO_2 were determined as about 342 and 475 nm respectively.

3.3. Fabrication of scaffolds

Histological studies were used to determine the most effective decellularization protocol, for which two main factors were important; more efficient cell removal and the least damage to the ECM. H&E staining of intact and decellularized specimens showed that trypsin/NaOH method resulted in the greatest cell removal (figure 2(1)) and specific stainings of collagen including Picro sirius red (figure 2(2)), Van Gieson (figure 2(3)) and Picro—indigo carmine (figure 2(4)) indicated the most preserved ECM structure using this method. The efficacy of cell removal using trypsin/NaOH method was further assessed by DAPI staining (figures 3(a) and (b)) and as seen in figure 3(b) the nuclei were removed effectively.

3.4. DNA content

Decellularization results were quantified by assessing DNA contents before and after cell removal using trypsin/NaOH method, which was selected as decellularization protocol based on histological studies. Comparing the optical densities of DNA samples extracted from intact and decellularized samples

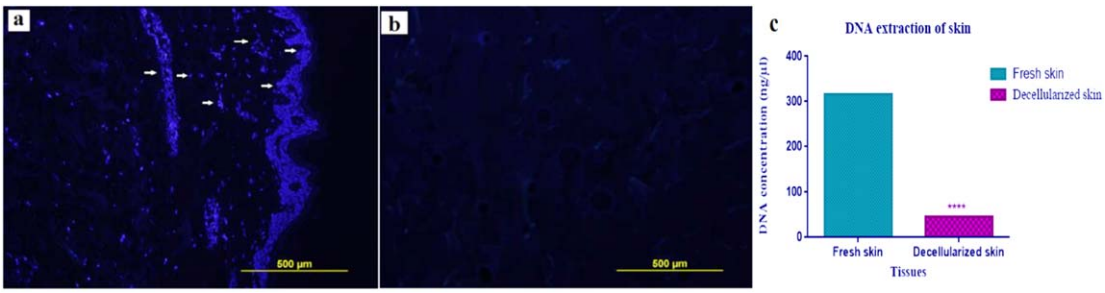

Figure 3. Confirming the efficacy of trypsin/NaOH method used for decellularization of human skin. DAPI staining (a) and (b) and DNA content analysis (c). In control fresh skin sample (a) the cell nuclei are seen as shining blue dots, and (b) indicates the sample after decellularization. (c) A decrease in DNA content from about 315–45 ng μl^{-1} indicates 85% DNA removal in decellularized sample relative to the fresh skin. Scale bar 500 μm. Mean $\pm$ standard deviation (SD).

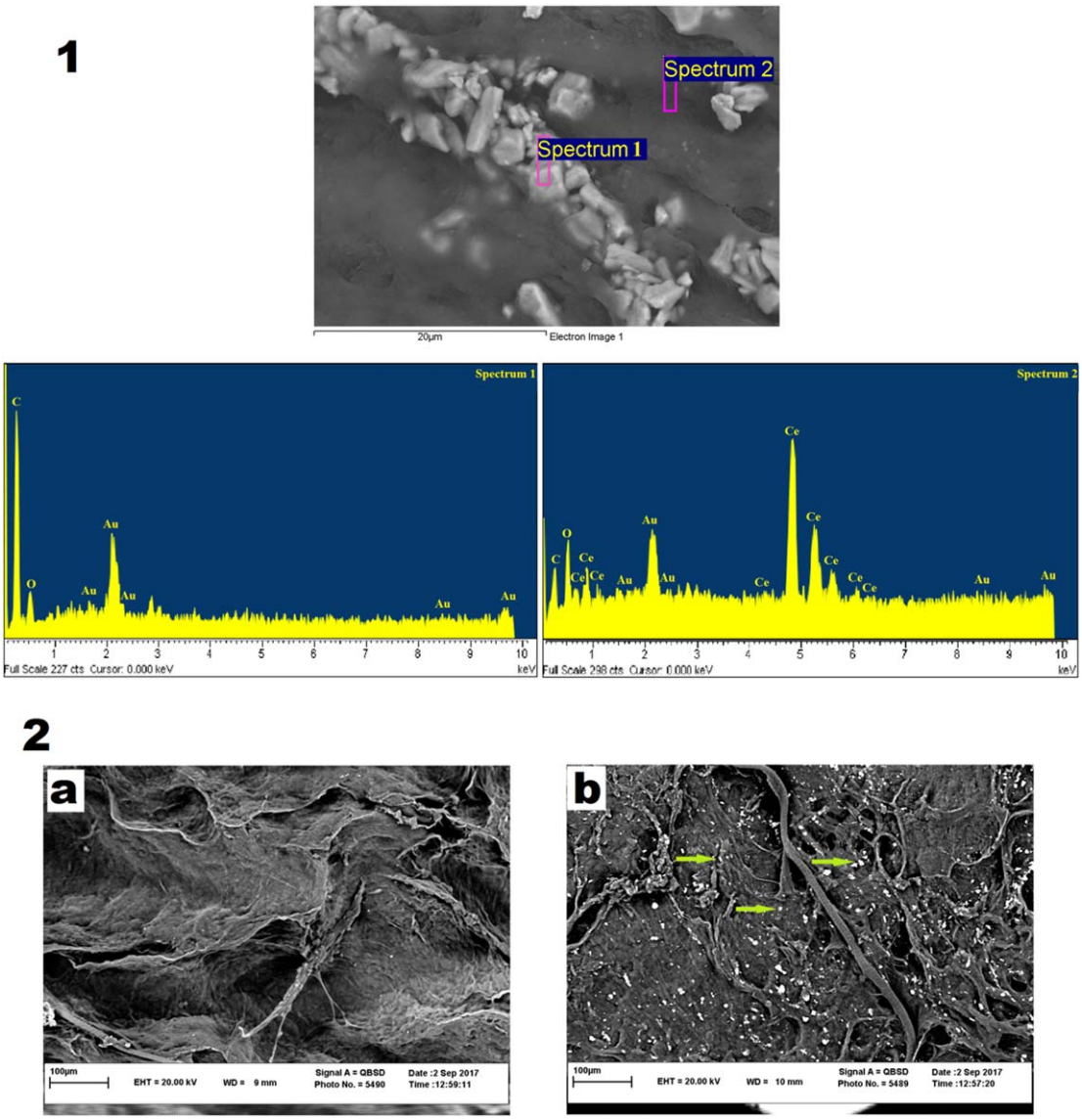

Figure 4. Confirmation of the nature of Ce on skin scaffolds loaded with CeO_2 nanoparticles by SEM. (1) A SEM micrograph of loaded scaffold in which two regions were selected and further analyzed by energy dispersive x-ray spectrometer analysis. In spectrum 1, the presence of carbon peaks reflects the organic nature of the matrix, while spectrum 2 confirms the presence of cerium element loaded on samples. (2) Backscattered electron images of a scaffold without nanoparticles (a) and a scaffold after immersion in nanoparticles (b). The arrows indicate the presence of CeO_2 nanoparticles on ADM after immersion in nanoparticles. Scale bar 100 μm.

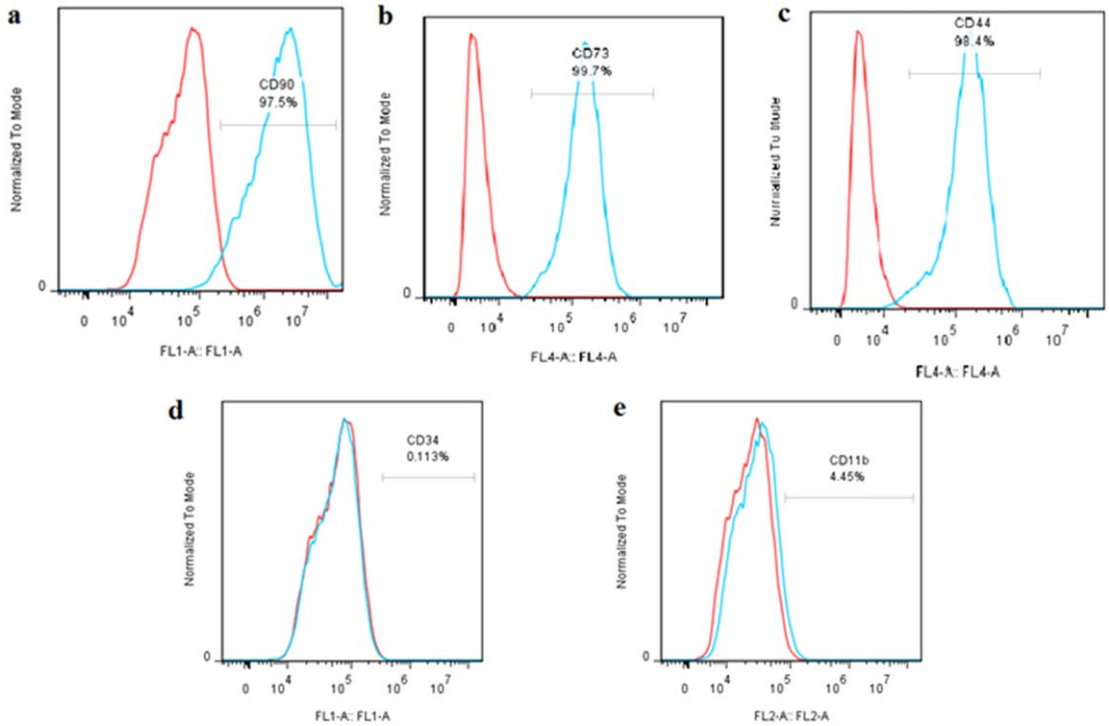

Figure 5. Flow cytometry analysis used for characterization of human Ad-MSCs. Results demonstrated that cells were mainly positive for the antigens CD90 (a), CD73 (b), CD44 (c) and negative for CD34 (d) and CD11b (e). ISO-FITC, ISO-PE and ISO-APC were considered as controls. (FITC: Fluorescein isothiocyanate; PE: phycoerythrin; APC: Allophycocyanin).

indicated 85% decrease in cellular remains after trypsin/NaOH treatment (figure 3(c)).

3.5. Cerium oxide nanoparticles loaded on ADM

The nature of the nanoparticles and their presence on the scaffolds were confirmed using a scanning electron microscope. As seen in figure 4(1), the Ce peaks obtained in spectrum 1 confirm the nature of cerium metal. While the C peaks recorded in spectrum 2 are related to the high carbon content of the scaffold. It should be noted that the Au peaks are related to gold, which was used for coating samples in preparation phase. Comparison between ADM and ADM/CeO_2 confirms that the scaffolds are impregnated with CeO_2 nanoparticles (figure 4(2)). The amount of nanoparticles taken up by the ADM was obtained from subtracting the photoluminescence data before and 24 h after immersing, as about 280 μg ml^{-1}.

3.6. Free radical scavenging

Antioxidant properties of decellularized samples (with and without CeO_2) were investigated by DPPH assay. DPPH is a stable free radical. Absorbance reduction at 517 nm and color change of the solution from purple to yellow is observed, when DPPH free radicals are scavenged by exposure to antioxidant agents. The results showed that DPPH degradation depends on CeO_2 concentration. The DPPH scavenging of ADM/CeO_2 with 0, 0.5, 1, 5 and 10 mg ml^{-1} of CeO_2 concentrations, were about 3.9%, 31.91%, 39.09%, 47.87% and 52.27%, respectively.

3.7. Characterization of hAd-MSCs

The expressions of specific cell surface antigens were investigated using flow cytometry (figure 5). These cells expressed the typical markers of MSCs (CD44, CD73, and CD90), while they were negative for CD34 and CD11b.

3.8. CeO_2 induced cell proliferation

The viability and growth of cultured hAd-MSCs in the presence of different concentrations of CeO_2 (figure 6(a)) and on ADM/CeO_2 (figures 6(b) and (c)) were evaluated by MTT assay. Results indicated that this nanoparticle has no toxicity on the cells. However, using 1.7×10^{-3} μg ml^{-1} (10^{-8} M) concentration of CeO_2 at 48 and 72 h increased the growth of these cells by 114% and 93% respectively. Moreover, in order to determine the optimal concentration for increasing the proliferation of cultured cells on ADMs, scaffolds were immersed in different concentrations of nanoparticle suspensions. MTT assay for various constructions on days 3, 7 and 14 indicated that use of 1 mg ml^{-1} CeO_2 resulted in the highest cell proliferation. MTT data also confirmed cell adhesion at 12 h and the increase in cell growth until day 14 after cell seeding. In this experiment, ADM/Ad-MSCs were considered as control groups.

H&E staining for ADM/hAd-MSCs and ADM/CeO_2/hAd-MSCs on days 3, 7 and 14 also showed increased number of cells in the presence of CeO_2 (figure 7(1)). SEM was utilized to assess the status of Ad-MSCs on the surface of the scaffolds in the

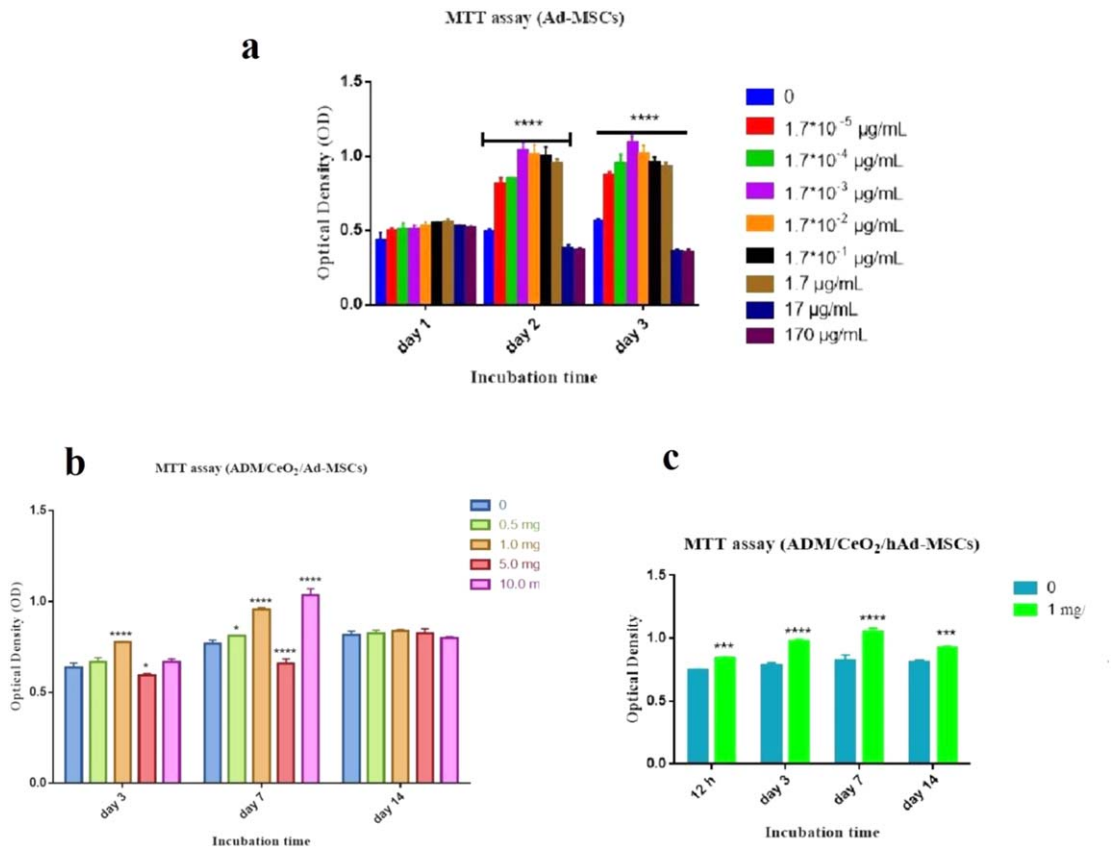

Figure 6. Investigating the effects of CeO_2 nanoparticles on viability of human Ad-MSCs by MTT assay. (a) Viability of Ad-MSCs following treatment with different concentrations of CeO_2 after 24, 48 and 72 h. As seen in the graph, after 24 h treatment, increasing CeO_2 concentration resulted to an increase in cell growth. At 48 and 72 h, the highest growth rates were related to the concentration of 1.7×10^{-3} μg ml^{-1} of CeO_2. (b) Viability and growth of Ad-MSCs seeded on ADM and ADM/CeO_2 using four different concentrations of CeO_2 nanoparticles were determined after 3, 7 and 14 d of incubation. (c) A significant increase was observed in Ad-MSC proliferation cultured on the scaffolds immersed in 1 mg ml^{-1} CeO_2 on days 3 and 7, data related to a biological repeat are shown as representative. Mean ± standard deviation (SD), $n = 3$, **** indicates $p < 0.0001$.

control and test samples. As shown in figure 7(2) the increase in the number and also attachment of the cultured cells onto the ADM/CeO_2 (figure 7(2)(b)) can clearly be observed in comparison to the control group (figure 7(2)(a)). The formation of pseudopodia in cultured cells on ADM/CeO_2 represents the stimulatory effects of this nanoparticle on cellular attachment and penetration.

3.9. Effects of CeO_2 on collagen density

Picro sirius red and Picro-indigo carmine stainings (figure 8) were used to evaluate the effects of CeO_2 on collagen density produced by the cells in the scaffolds. Increasing in collagen density was observed in ADM/CeO_2/hAd-MSCs compared to ADM/hAd-MSCs. SEM images also represented the structure of the scaffolds after exposure to CeO_2. These images confirm the higher density of scaffold collagens after treatment with CeO_2 (figure 9(1)). In addition, TEM images (figure 9(2)) confirm these results and indicated the maintenance of collagen fibrils alignment even after collagen deposition in ADM/CeO_2/hAd-MSCs which changed orientation of these fibrils at day 14.

3.10. CeO_2 increased tensile strength

The composition and organization of the ECM can affect the biomechanical properties of the skin. In this study, various treatments were performed on the skin which may change the ECM structure. So, ultimate tensile strength (UTS) as a mechanical property was evaluated as shown in table 2. Results indicated that biomechanical properties of the samples changed during the 2 weeks time of the experiment. In all three time points ADM/CeO_2/Ad-MSCs had a maximum ultimate tensile load at failure (N). Based on these data, it can be concluded that cells and CeO_2 nanoparticles, as well as time, have improved mechanical properties of the ADM probably through changing the structure of the ECM.

4. Discussion

The purpose of the skin tissue engineering is to achieve a skin substitute, which can be successfully transplanted and to form a grainy tissue, capable of angiogenesis and re-epithelialization [35]. Reports on Ad-MSCs have shown the differentiation potential of these cells into fibroblast-like cells [36], as well as

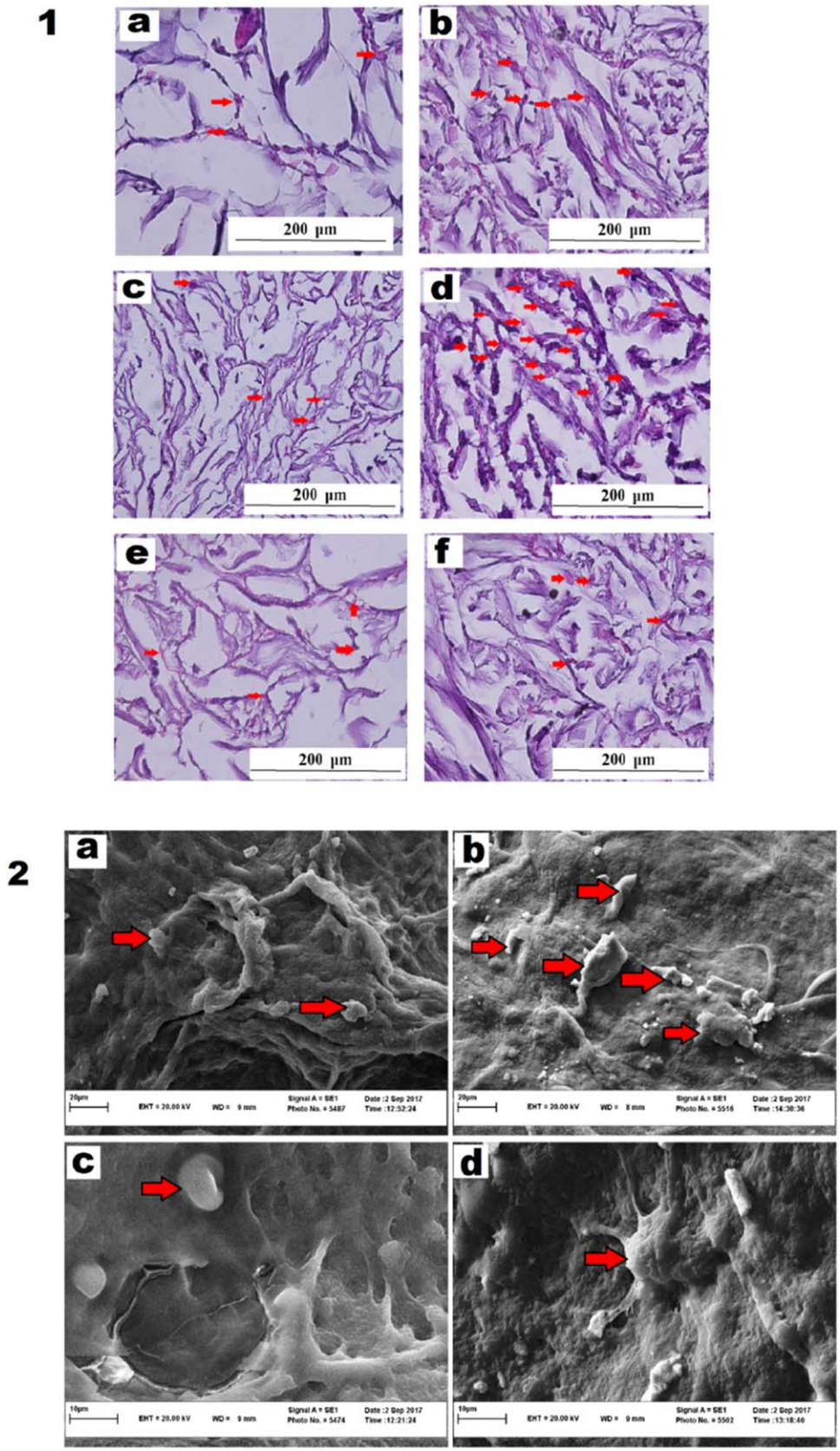

Figure 7. Effects of CeO_2 incubation time on Ad-MSCs seeded on ADM. (1) Skin scaffolds seeded with Ad-MSCs in absence (a), (c), (e) or presence (b), (d) and (f) of CeO_2 nanoparticles were stained with H&E after 3 (a), (b), 7 (c), (d) and 14 (e), (f) days of culture. Cells are indicated with arrows and an increase in cell number is observed in nanoparticle-coated scaffolds as compared to the controls. The presence of cells in e and f demonstrates cell survival until day 14. (2) Presence of cells was also confirmed by SEM (a and b $\times 2000$, c and d $\times 5000$). Morphology of Ad-MSCs cultured on ADM (a), (c) is compared with cells grown on ADM/CeO_2 (b), (d) after 10 days of culture. Increased number of cells, as well as morphological changes can be observed relative to controls, indicating inducing effects of CeO_2 on proliferation and penetration of Ad-MSCs into the scaffolds. Creation of pseudopodia and cell adhesion to the scaffolds coated with CeO_2 is shown in d. Scale bar: (1) 200 μm; 2 (a), (b) 20 μm; 2 (c), (d) 10 μm.

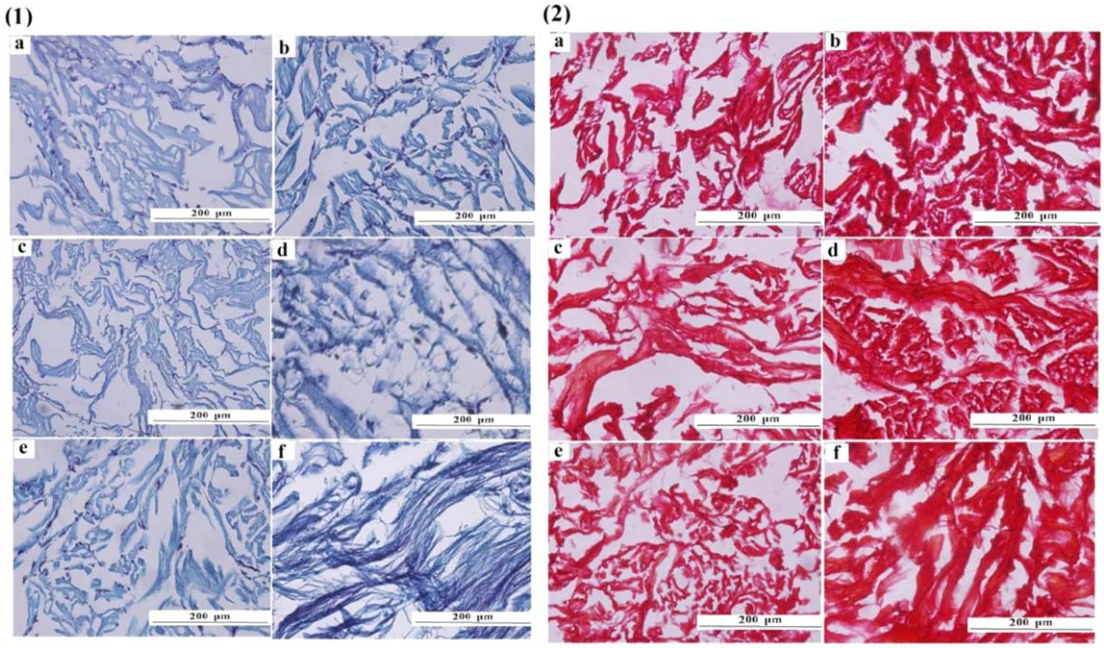

Figure 8. Histological analysis showing the effects of CeO_2 on collagen density. Histological analysis of ADM/Ad-MSCs (a), (c) and (e) and ADM/CeO_2/Ad-MSCs (b, d and f) at days 3 (a), (b), 7 (c), (d) and 14 (e), (f) as stained with Picro indigo carmine (1) and Picro sirius red (2). Increasing the color intensity of ADM/CeO_2/Ad-MSCs confirms the increase in the density and diameter of collagen fibers. Scale bar 200 μm.

stimulation of collagen synthesis and angiogenesis in the injured skin [37]. Cultivation of Ad-MSCs on ADM is reported as one strategy to accelerate wound healing by many investigators. However, the method used for preparation of ADM is important to facilitate the attachment, viability and differentiation of cultured cells. For ADM preparation, in this study human skin samples harvested after liposuction surgeries were decellularized using four different protocols. The results of histological studies and DNA extraction confirmed the suitability of the trypsin/NaOH method as shown in the previous studies [32]. It is undeniable that every decellularization method will alter ECM structure though to a different degree. Although, NaOH and trypsin promote cell removal process, they may disrupt collagen fibers and other ECM components [38].

New concepts in skin tissue engineering offer special needs for biomimetic scaffolds. Nanomaterials can be used to enhance tissue and organ regeneration by affecting cellular behavior. However, optimization of dispersion methods should be considered as an important factor affecting their biological properties [39]. In this study, different methods of dispersion were investigated and it was finally determined that wetting with FBS can increase the stability of the suspension. Since the interaction between the nanoparticles and the hydrophilicproteins prevents their agglomeration, stabilization of the suspension is predictable after addition of FBS. Moreover, previous studies have shown the role of FBS in the stability of nanoparticle suspensions [40, 41]. It has been shown that CeO_2 nanoparticles stimulate the growth and proliferation of normal cells [42]. These nanoparticles also accelerated wound healing process and angiogenesis [43]. In this study, the toxicity of CeO_2 on hAd-MSCs was evaluated using MTT assay in three days of culture. Our results indicated that this nanoparticle not only had no toxicity on cells but also induced their proliferation at optimized concentrations. However, due to NPs agglomeration and deposition, high concentrations of CeO_2 nanoparticles (170 and 17 μg ml^{-1}) led to a significant decrease in proliferation rate on days 2 and 3. These negative effects may depend on the mechanisms of CeO_2 nanoparticles uptake by cells and subsequently their pH-dependent antioxidant activity. The aggregated nanoparticles penetrate into cells through clathrin-dependent endocytosis, and cannot directly pass through cell membrane as is the case for monodispersed CeO_2 nanoparticles [42]. So these nanoparticles ultimately localized in lysosomes (acidic pH) can cause accumulation of free radicals and production of H_2O_2 which is toxic for cells [44].

In order to have an efficient skin tissue engineering, in this study various concentrations of CeO_2 nanoparticles (0.5, 1, 5 and 10 mg ml^{-1}) were loaded onto hADMs, followed by culture of hAd-MSCs on these constructs for two weeks. Increased growth and proliferation of cells was observed at the concentration of 1 mg ml^{-1} as compared with untreated groups. The results of antioxidant assays for scaffolds showed a concentration-dependent trend for antioxidant effects of CeO_2. Although physiological levels of reactive oxygen species (ROS) are essential for different steps of

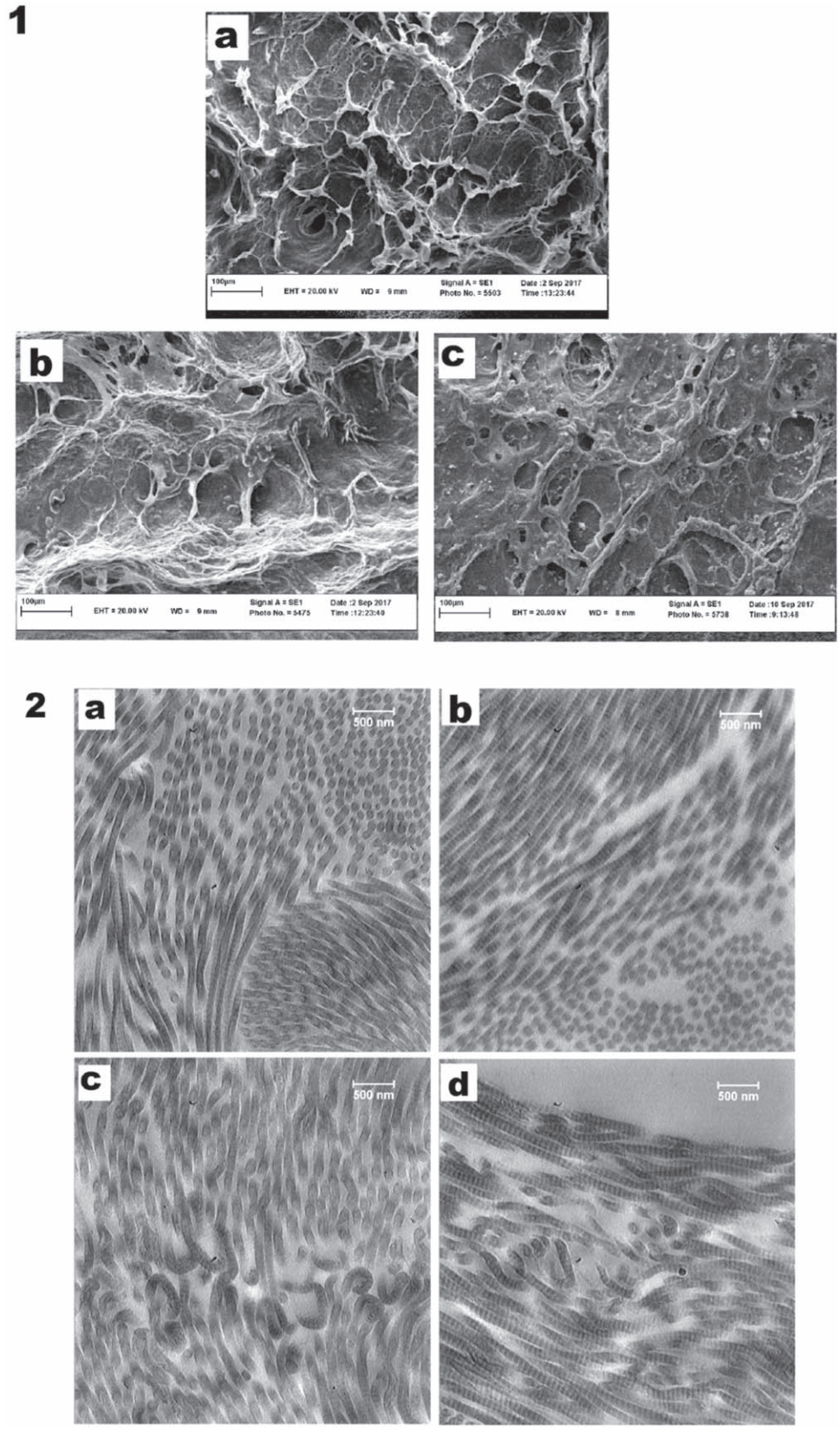

Figure 9. SEM and TEM micrographs showing the effects of CeO_2 on collagen density. (1): Representative SEM micrographs of ADM ×500 (a) ADM/Ad-MSCs (b) and ADM/CeO_2/Ad-MSCs (c). Increasing collagen density in (b) compared with (a) shows the production of collagen by Ad-MSCs, and increased density of collagen in (c) compared to (b) shows the inducing effects of CeO_2 on collagen production. In addition, TEM micrographs ×4000 (2) show orientation, alignment and deposition of collagen fibrils in ADM/Ad-MSCs (a), (b) ADM/CeO_2/Ad-MSCs (c), (d) at days 7 (a), (c) and 14 (b), (d). These images show that the alignment of the fibers in the presence of CeO_2 is preserved until day 14. Moreover, the arches at the junction of fibers confirm the fibrous tissue and their altered orientation due to the difference in regional mechanics. Scale bar: SEM 100 μm; TEM 500 nm.

Table 2. The effects of Ad-MSCs and CeO_2 nanoparticles on the mechanical properties of ADM.

Test specimen sample name	Force (N)	Extension (mm)	Module (MPa)
ADM 3	6.66	13.38	0.29
ADM 7	15.32	12.82	0.7
ADM 14	16.54	10.10	2.76
ADM/Ad-MSCs 3	38.33	18.16	1.3
ADM/Ad-MSCs 7	44.92	11.09	2.05
ADM/Ad-MSCs 14	57.79	12.38	2.79
ADM/CeO_2/Ad-MSCs 3	53	19.94	1.7
ADM/CeO_2/Ad-MSCs 7	66.83	13.65	2.42
ADM/CeO_2/Ad-MSCs 14	115.49	9.26	7.47

wound healing [45], its excessive reduction which occurs at high concentrations (5 and 10 mg ml^{-1}) of cerium, can result to a decrease in cell proliferation. Furthermore, histological images and SEM confirmed the stimulatory effects of CeO_2 on growth and cell proliferation. Moreover, as evidenced by histological stainings, SEM and TEM, when the combination of ADM/CeO_2/Ad-MSCs was used, collagen production and deposition were increased in the presence of nanoparticles. It has been shown that expression and deposition of collagen are associated with increased levels of transforming growth factor β (TGFβ) [46–48]. This factor is secreted by fibroblasts in the wound healing process. In addition, it can also be produced by Ad-MSCs. So, it can be concluded that this factor might be secreted either by the stem cells or less probably fibroblasts produced by differentiation of Ad-MSCs on the scaffolds. Collagen is important in cell-ECM interactions and cellular adhesion and migration [49]. On the other hand, in the wound healing process, it is shown that due to reduction of tensile strength, regeneration time is longer, but using collagen sponge, the parallel deposition of newly synthesized collagen fibrils can be promoted. Thus, the tissue increase in the tensile strength resulted in faster recovery [50]. The tensile strength comparison between ADM, ADM/Ad-MSCs and ADM/CeO_2/Ad-MSCs confirmed the effective impacts of CeO_2 on the scaffolds mechanical properties. As shown in TEM images, in this study collagen fibrils in ADM/CeO_2/
hAd-MSCs have been deposited in a parallel alignment. Collagen fibril arches on day 14 confirm the alteration of the collagen fibers to fibrosis structure. Although these structures are organized in wound healing process by fibroblasts, we have shown that these arches were created *in vitro* for the first time. Since matrix fibrillation affects cell proliferation, the reduced cell growth observed on day 14, might be due to this fibrillation. In spite of reduced cell growth at day 14, due to the uniaxial stretch and rotation, alignment and straightness of collagen in the direction of this stretch, the tensile strength will increase as shown by mechanical test in our study. Ultimately, the data reported in this study indicate the potential of this constructions containing ADM scaffolds, CeO_2 nanoparticles and Ad-MSCs as a better approach for skin regenerative medicine [50].

5. Conclusion

Our results showed that trypsin/NaOH protocol had the lowest damage to the ECM as compared to other protocols used for decellularization in this study. Among different dispersal methods, the approach using DMEM medium, wetting with FBS and using ultrasonic bath resulted in the best stability of CeO_2 suspension. The MTT assay indicated that CeO_2 not only had no toxicity on the cells, but also increased the growth and survival of hAd-MSCs at a certain concentration. Moreover, antioxidant and mechanical tests and also histological studies confirmed enhancing effects of CeO_2 on proliferation and survival of hAd-MSCs as well as the amount of collagen in the scaffolds. In summary, it can be concluded that the combination of ADM/CeO_2/hAd-MSCs could be a step forward in skin tissue engineering, however, more studies on animal models are required to confirm these results.

Acknowledgments

The authors would like to acknowledge IRAN Nanotechnology Initiative Council (INIC) and Central Laboratory of Ferdowsi University of Mashhad for their technical supports and also thank Prof. Bahrami for his financial supports. We are also grateful to Mr Mirahmadi, Mr Zahabi and Mr Nakhaei for their technical assistance. This research was funded by a grant from Ferdowsi University of Mashhad (42511).

Funding

This study was funded by a grant (no 42511) from Ferdowsi University of Mashhad, Iran.

ORCID iDs

Maryam M Matin https://orcid.org/0000-0002-7949-7712

References

[1] Bielefeld K A, Amini-Nik S and Alman B A 2013 Cutaneous wound healing: recruiting developmental pathways for regeneration *Cell Mol. Life Sci.* **70** 2059–81

[2] Greenwood H L, Singer P A, Downey G P, Martin D K, Thorsteinsdottir H and Daar A S 2006 Regenerative medicine and the developing world *PLoS Med.* **3** e381

[3] Than P A, Davis C R and Gurtner G C 2016 Clinical management of wound healing and hypertrophic scarring *Skin Tissue Engineering and Regenerative Medicine* (New York: Academic) pp 61–81

[4] Dieckmann C, Renner R, Milkova L and Simon J C 2010 Regenerative medicine in dermatology: biomaterials, tissue engineering, stem cells, gene transfer and beyond *Exp. Dermatol.* **19** 697–706

[5] Metcalfe A D and Ferguson M W 2007 Tissue engineering of replacement skin: the crossroads of biomaterials, wound healing, embryonic development, stem cells and regeneration *J. R. Soc. Interface* **4** 413–37

[6] Kokai L E, Marra K and Rubin J P 2014 Adipose stem cells: biology and clinical applications for tissue repair and regeneration *Transl. Res.* **163** 399–408

[7] Derwin K A, Badylak S F, Steinmann S P and Iannotti J P 2010 Extracellular matrix scaffold devices for rotator cuff repair *J. Shoulder Elbow Surg.* **19** 467–76

[8] Reing J E, Zhang L, Myers-Irvin J, Cordero K E, Freytes D O, Heber-Katz E, Bedelbaeva K, McIntosh D, Dewilde A and Braunhut S J 2008 Degradation products of extracellular matrix affect cell migration and proliferation *Tissue Eng.* A **15** 605–14 -

[9] Macadam S A and Lennox P A 2012 Acellular dermal matrices: use in reconstructive and aesthetic breast surgery *Can. J. Plast. Surg.* **20** 75–89

[10] Chaudhury K, Kumar V, Kandasamy J and RoyChoudhury S 2014 Regenerative nanomedicine: current perspectives and future directions *Int. J. Nanomed.* **9** 4153–67

[11] Choi H S and Frangioni J V 2010 Nanoparticles for biomedical imaging: fundamentals of clinical translation *Mol. Imaging* **9** 291–310

[12] Korsvik C, Patil S, Seal S and Self W T 2007 Superoxide dismutase mimetic properties exhibited by vacancy engineered ceria nanoparticles *Chem. Commun.* **10** 1056–8

[13] Pezzini I, Marino A, Del Turco S, Nesti C, Doccini S, Cappello V and Ciofani G 2017 Cerium oxide nanoparticles: the regenerative redox machine in bioenergetic imbalance *Nanomedicine* **12** 403–16

[14] Hirst S M, Karakoti A S, Tyler R D, Sriranganathan N, Seal S and Reilly C M 2009 Anti-inflammatory properties of cerium oxide nanoparticles *Small* **5** 2848–56

[15] Chen J, Patil S, Seal S and McGinnis J F 2006 Rare earth nanoparticles prevent retinal degeneration induced by intracellular peroxides *Nat. Nanotechnol.* **1** 142–50

[16] Tarnuzzer R W, Colon J, Patil S and Seal S 2005 Vacancy engineered ceria nanostructures for protection from radiation-induced cellular damage *Nano Lett.* **5** 2573–7

[17] Colon J, Herrera L, Smith J, Patil S, Komanski C, Kupelian P, Seal S, Jenkins D W and Baker C H 2009 Protection from radiation-induced pneumonitis using cerium oxide nanoparticles *Nanomed.: Nanotechnol., Biol. Med.* **5** 225–31

[18] Das S, Singh S, Dowding J M, Oommen S, Kumar A, Sayle T X, Saraf S, Patra C R, Vlahakis N E and Sayle D C 2012 The induction of angiogenesis by cerium oxide nanoparticles through the modulation of oxygen in intracellular environments *Biomaterials* **33** 7746–55

[19] Chigurupati S, Mughal M R, Okun E, Das S, Kumar A, McCaffery M, Seal S and Mattson M P 2013 Effects of cerium oxide nanoparticles on the growth of keratinocytes, fibroblasts and vascular endothelial cells in cutaneous wound healing *Biomaterials* **34** 2194–201

[20] Karakoti A S, Tsigkou O, Yue S, Lee P D, Stevens M M, Jones J R and Seal S 2010 Rare earth oxides as nanoadditives in 3D nanocomposite scaffolds for bone regeneration *J. Mater. Chem.* **20** 8912–9

[21] Davan R, Prasad R, Jakka V S, Aparna R, Phani A, Jacob B, Salins P C and Raju D 2012 Cerium oxide nanoparticles promotes wound healing activity in *in-vivo* animal model *J. Bionanosci.* **6** 78–83

[22] Das M, Patil S, Bhargava N, Kang J-F, Riedel L M, Seal S and Hickman J J 2007 Auto-catalytic ceria nanoparticles offer neuroprotection to adult rat spinal cord neurons *Biomaterials* **28** 1918–25

[23] Cimini A, D'Angelo B, Das S, Gentile R, Benedetti E, Singh V, Monaco A M, Santucci S and Seal S 2012 Antibody-conjugated PEGylated cerium oxide nanoparticles for specific targeting of Aβ aggregates modulate neuronal survival pathways *Acta Biomater.* **8** 2056–67

[24] Decoteau W E, Heckman K, Reed K and Erlichman J S 2012 Ceria nanoparticles reduce disease severity in a mouse model of multiple sclerosis *In TechConnect World Conf. and Expo.* vol 3 pp 265–8

[25] Kim C K, Kim T, Choi I Y, Soh M, Kim D, Kim Y J, Jang H, Yang H S, Kim J Y, Park H K, Park S P, Park S, Yu T, Yoon B W, Lee S H and Hyeon T 2012 Ceria nanoparticles that can protect against ischemic stroke *Angew. Chem., Int. Ed.* **51** 11039–43

[26] Alili L, Sack M, Karakoti A S, Teuber S, Puschmann K, Hirst S M, Reilly C M, Zanger K, Stahl W and Das S 2011 Combined cytotoxic and anti-invasive properties of redox-active nanoparticles in tumor–stroma interactions *Biomaterials* **32** 2918–29

[27] Alili L, Sack M, Von Montfort C, Giri S, Das S, Carroll K S, Zanger K, Seal S and Brenneisen P 2013 Downregulation of tumor growth and invasion by redox-active nanoparticles *Antioxid. Redox Signal.* **19** 765–78

[28] Giri S, Karakoti A, Graham R P, Maguire J L, Reilly C M, Seal S, Rattan R and Shridhar V 2011 Nanoceria: a rare-earth nanoparticle as a novel anti-angiogenic therapeutic agent in ovarian cancer *PLoS One* **8** e54578

[29] Charbgoo F, Ahmad M B and Darroudi M 2017 Cerium oxide nanoparticles: green synthesis and biological applications *Int. J. Nanomed.* **12** 1401–13

[30] Boone M A, Draye J P, Verween G, Aiti A, Pirnay J P, Verbeken G, De Vos D, Rose T, Jennes S and Jemec G B 2015 Recellularizing of human acellular dermal matrices imaged by high-definition optical coherence tomography *Exp. Dermatol.* **24** 349–54

[31] Reing J E, Brown B N, Daly K A, Freund J M, Gilbert T W, Hsiong S X, Huber A, Kullas K E, Tottey S and Wolf M T 2010 The effects of processing methods upon mechanical and biologic properties of porcine dermal extracellular matrix scaffolds *Biomaterials* **31** 8626–33

[32] Zhang X, Deng Z, Wang H, Yang Z, Guo W, Li Y, Ma D, Yu C, Zhang Y and Jin Y 2009 Expansion and delivery of human fibroblasts on micronized acellular dermal matrix for skin regeneration *Biomaterials* **30** 2666–74

[33] Selvaraj S and Fathima N N 2017 Fenugreek incorporated silk fibroin nanofibers—a potential antioxidant scaffold for enhanced wound healing *ACS Appl. Mater. Interfaces* **9** 5916–26

[34] Ahmadian kia N, Bahrami A R, Ebrahimi M, Matin M M, Neshati Z, Almohaddesin M R, Aghdami N and Bidkhori H R 2011 Comparative analysis of chemokine receptor's expression in mesenchymal stem cells derived from human bone marrow and adipose tissue *J. Mol. Neurosci.* **44** 178–85

[35] Altman A M, Matthias N, Yan Y, Song Y-H, Bai X, Chiu E S, Slakey D P and Alt E U 2008 Dermal matrix as a carrier for *in vivo* delivery of human adipose-derived stem cells *Biomaterials* **29** 1431–42

[36] Hur W, Lee H Y, Min H S, Wufuer M, Lee C W, Hur J A, Kim S H, Kim B K and Choi T H 2017 Regeneration of full-thickness skin defects by differentiated adipose-derived stem cells into fibroblast-like cells by fibroblast-conditioned medium *Stem Cell Res. Ther.* **8** 92

[37] Orbay H, Takami Y, Hyakusoku H and Mizuno H 2011 Acellular dermal matrix seeded with adipose-derived stem cells as a subcutaneous implant *Aesthetic Plast. Surg.* **35** 756–63
[38] Crapo P M, Gilbert T W and Badylak S F 2011 An overview of tissue and whole organ decellularization processes *Biomaterials* **32** 3233–43
[39] Kumar A, Das S, Munusamy P, Self W, Baer D R, Sayle D C and Seal S 2014 Behavior of nanoceria in biologically-relevant environments *Environ. Sci.: Nano* **1** 516–32
[40] Casals E, Pfaller T, Duschl A, Oostingh G J and Puntes V 2010 Time evolution of the nanoparticle protein corona *ACS Nano* **4** 3623–32
[41] Sharma G, Kodali V, Gaffrey M, Wang W, Minard K R, Karin N J, Teeguarden J G and Thrall B D 2014 Iron oxide nanoparticle agglomeration influences dose rates and modulates oxidative stress-mediated dose–response profiles *in vitro Nanotoxicology* **8** 663–75
[42] Popov A L, Popova N R, Selezneva I I, Akkizov A Y and IvanovV K 2016 Cerium oxide nanoparticles stimulate proliferation of primary mouse embryonic fibroblasts *in vitro Mater. Sci. Eng.* C **68** 406–13
[43] Zgheib C, Hilton S A, Dewberry L C, Hodges M M, Ghatak S, Xu J, Singh S, Roy S, Sen C K and Seal S 2019 Use of cerium oxide nanoparticles conjugated with microRNA-146a to correct the diabetic wound healing impairment *J. Am. Coll. Surg.* **228** 107–15
[44] Perez J M, Asati A, Nat S and Kaittanis C 2008 Synthesis of biocompatible dextran-coated nanoceria with pH-dependent antioxidant properties *Small* **4** 552–6
[45] Rather H A, Thakore R, Singh R, Jhala D, Singh S and Vasita R 2018 Antioxidative study of cerium oxide nanoparticle functionalised PCL-Gelatin electrospun fibers for wound healing application *Bioact. Mater.* **3** 201–11
[46] Van Bruaene N, Derycke L, Perez-Novo C A, Gevaert P, Holtappels G, De Ruyck N, Cuvelier C, Van Cauwenberge P and Bachert C 2009 TGF-β signaling and collagen deposition in chronic rhinosinusitis *J. Allergy Clin. Immunol.* **124** e252
[47] Lawrance I C, Maxwell L and Doe W 2001 Inflammation location, but not type, determines the increase in TGF-β1 and IGF-1 expression and collagen deposition in IBD intestine *Inflamm. Bowel Dis.* **7** 16–26
[48] Chakir J, Shannon J, Molet S, Fukakusa M, Elias J, Laviolette M, Boulet L-P and Hamid Q 2003 Airway remodeling-associated mediators in moderate to severe asthma: effect of steroids on TGF-β, IL-11, IL-17, and type I and type III collagen expression *J. Allergy Clin. Immunol.* **111** 1293–8
[49] Farndale R W, Lisman T, Bihan D, Hamaia S, Smerling C S, Pugh N, Konitsiotis A, Leitinger B, de Groot P G and Jarvis G E 2008 Cell–collagen interactions: the use of peptide toolkits to investigate collagen–receptor interactions *Biochem. Soc. Trans.* **36** 241–50
[50] Sander E A, Lynch K A and Boyce S T 2014 Development of the mechanical properties of engineered skin substitutes after grafting to full-thickness wounds *J. Biomech. Eng.* **136** 051008